

ABEL-FRET: tether-free single-molecule FRET with hydrodynamic profiling

Hugh Wilson^{id} and Quan Wang^{id}

Single-molecule Förster resonance energy transfer (smFRET) has become a versatile and widespread method to probe nanoscale conformation and dynamics. However, current experimental modalities often resort to molecule immobilization for long observation times and do not always approach the resolution limit of FRET-based nanoscale metrology. Here we present ABEL-FRET, an immobilization-free platform for smFRET measurements with ultrahigh resolving power in FRET efficiency. Importantly, single-molecule diffusivity is used to provide additional size and shape information for hydrodynamic profiling of individual molecules, which, together with the concurrently measured intramolecular conformation through FRET, enables a holistic and dynamic view of biomolecules and their complexes.

Since the pioneering work by Ha et al.¹, smFRET has evolved into a powerful tool across physical chemistry, biophysics and molecular biology (see the recent review by Lerner et al.² and the references within). Nevertheless, the current technology has limitations: for long observation times, many smFRET measurements attach biomolecules to a surface³, a practice that might not be feasible or desirable for some samples⁴. Moreover, a single one-dimensional readout of FRET efficiency is often not enough to capture the full complexity of biological systems, especially in the presence of biomolecular interactions. We present ABEL-FRET, a tether-free platform for continuous monitoring of smFRET over several seconds with ultrahigh resolution of structural heterogeneity. Because the molecule of interest is untethered and free to move in solution, its hydrodynamic properties can be measured simultaneously to give additional access to the size, shape, stoichiometric composition and binding state of biomolecular complexes. This provides a valuable extra dimension, in addition to intramolecular conformation from smFRET, for dissecting biomolecular processes.

ABEL-FRET combines the anti-Brownian electrokinetic (ABEL) trap⁵, a platform for isolating individual molecules in solution, with photon-counting smFRET detection optics^{6,7} (Fig. 1a). To capture single molecules in aqueous solution, the ABEL trap monitors the target molecule's position in real time and applies electrokinetic feedback to approximately cancel the molecule's Brownian motion. We implemented an advanced version of the ABEL trap using rapid beam scanning, optimal real-time signal processing, fused silica microfluidic sample chambers⁸ and added dual-channel photon counting for FRET detection (Supplementary Fig. 1, Supplementary Note 1 and Supplementary Software). This apparatus allowed smFRET to be measured photon-by-photon over many seconds in solution, without tethering (Fig. 1b). In addition, building on recently developed trajectory analysis of the trapped molecule's residual stochastic motion, the diffusion coefficient (D) of the molecule was simultaneously⁹ measured to provide hydrodynamic information.

Results

To characterize the performance of ABEL-FRET and allow comparison with conventional smFRET modalities, we first quantify the ability to resolve different species in FRET efficiency (E_{FRET}) space.

In practice, the resolving power is determined by the width of the efficiency histogram of a single static FRET population. This width is bounded by the fundamental statistics of photon counting (that is the shot-noise limit)¹⁰. To test whether ABEL-FRET reaches the shot-noise limit, we measured 11-base-pair (bp) DNA duplexes end-labeled with a Cy3–Cy5 pair and characterized the standard deviation of the FRET efficiency histogram versus the number of photons (N) used per E_{FRET} calculation (Extended Data Fig. 1). We expect the short DNA duplex to display constant E_{FRET} at the timescale of our efficiency calculations. We found that the histogram width scales as $1/\sqrt{N}$, as expected for a shot-noise limited measurement, and approaches the absolute value of the shot-noise limit (Supplementary Notes 2 and 3) within 30%, when the analysis was performed on either a single molecule or data pooled from 226 molecules (Extended Data Fig. 1c). Notably, our efficiency histograms are several-fold narrower compared to literature values from conventional smFRET modalities^{11–14} (Extended Data Fig. 1d and Supplementary Note 4). Further, we demonstrated that narrow smFRET distributions ($\sigma \approx 0.026$) can also be obtained on dual-labeled proteins (here using adenylate kinase¹⁵ as a model system, Extended Data Fig. 2).

The narrower widths observed for a single static species suggest that ABEL-FRET will improve the power to resolve multiple closely spaced FRET populations. To explore the practical limit of resolution, we challenged ABEL-FRET to resolve a mixture of 13 different short DNA duplexes in a single experiment. In this case, the molecules are all labeled at the ends and differ by only 1 or 2 bp (Supplementary Table 2). Static heterogeneity at this level was challenging to resolve in previous smFRET attempts¹¹. We trapped molecules in the mixture one by one and built a FRET efficiency histogram from 1,477 molecules (Fig. 1c and Extended Data Fig. 3). ABEL-FRET clearly resolves 12 distinct populations with the possibility to resolve more near the ends of the efficiency range (that is $E < 0.15$ and $E > 0.8$). This is a large number (12) of static FRET populations resolved in a single experiment and a high resolving power ($\Delta E \approx 0.02$ between 19 and 20 bp) demonstrated with smFRET. Note that this ultrahigh resolving power was achieved with a typical number of photons (an average of 25,200 photons per molecule) on the commonly used Cy3–Cy5 pair. We also showed that with as few as 1,000 photons (or 65-ms time resolution under

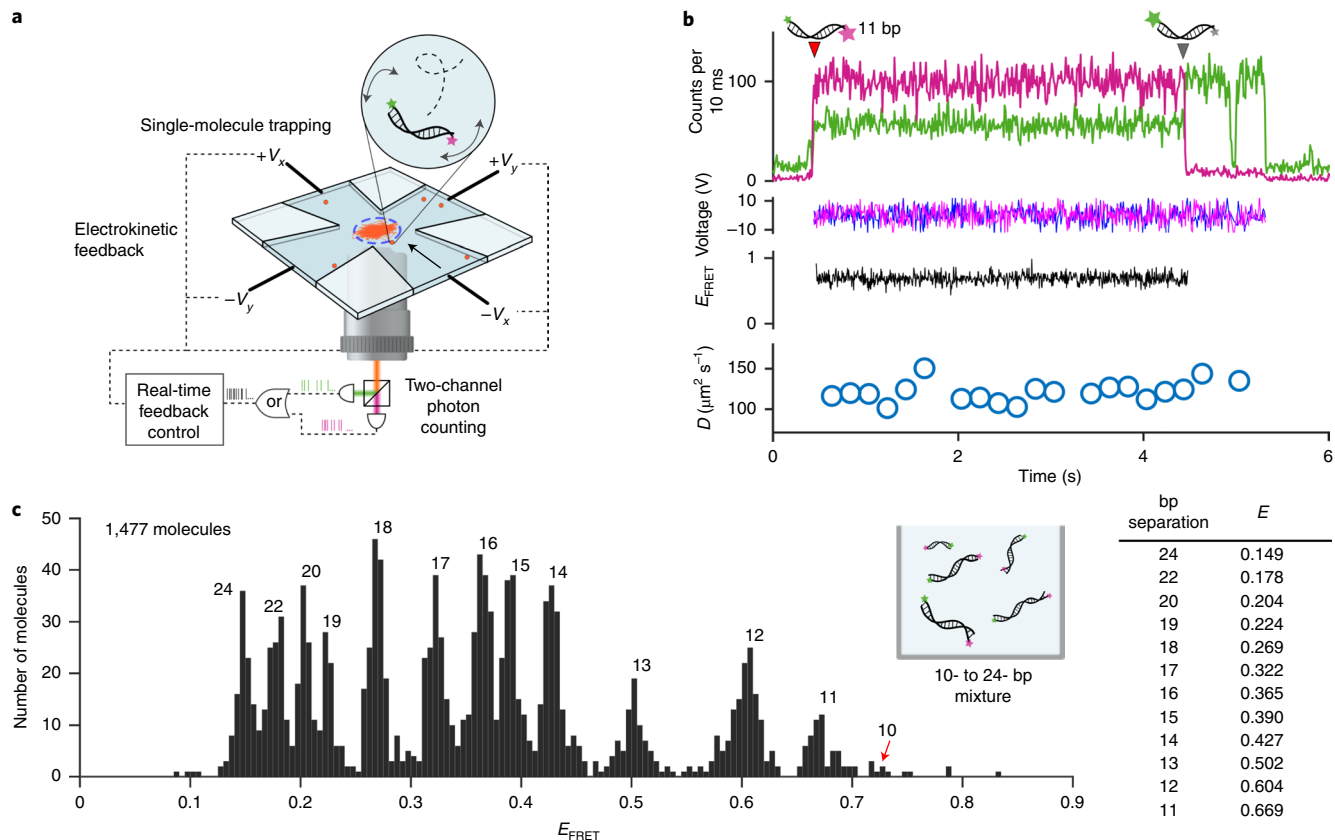


Fig. 1 | ABEL-FRET combines feedback trapping with two-color photon counting to enable tether-free smFRET in solution and ultrahigh resolution of structural mixtures. **a**, Overview of ABEL-FRET apparatus (see Supplementary Fig. 1 for details). $+V_x$, $+V_y$, $-V_x$, and $-V_y$ indicate the four electrodes used for feedback trapping. **b**, An example measurement trace on 11-bp DNA, showing fluorescence intensity of donor (green) and acceptor (red) channels (10-ms bins), feedback voltages for trapping, FRET efficiency (10-ms bins) and estimated diffusion coefficient (200-ms bins). **c**, Resolving a 13-component mixture of short DNA duplexes using FRET efficiency. The numbers of base pairs are noted at the top of the identified populations. The 10-bp dsDNA was not well-resolved (red arrow), likely due to dissociation during the course of the experiment. Mean FRET efficiencies of the 12 resolvable species are tabulated. A mean of 25,200 photons (median, 19,100 photons) were detected per molecule.

our experimental conditions), single base-pair resolution on DNAs can be achieved (Supplementary Fig. 3), suggesting the improved resolving power would benefit dynamic systems as well. The resolving power demonstrated here on static ensembles of similar molecules paves the way for future experiments aimed at uncovering high-resolution structural details of individual biomolecules.

We next demonstrate continuous monitoring of smFRET dynamics over a range of timescales without tethering. First, we measured the spontaneous interconversion between the two stacked isomers of the Holliday junction (HJ)¹⁶. With ABEL-FRET, transitions between two FRET levels were clearly visualized (Fig. 2a and Supplementary Fig. 4). Magnesium-dependent isomerization rates (from ~ 10 to $\sim 500\text{ s}^{-1}$) were extracted through photon-by-photon cross-correlation analysis and agree with previous measurements on immobilized molecules (Extended Data Fig. 4)¹⁶. Furthermore, observation that kinetic rates are independent of the feedback strength (Supplementary Fig. 5) alleviated the concern that the feedback electric fields might perturb HJ behavior (Supplementary Note 6). We next measured smFRET dynamics from single-stranded DNA (ssDNA)-binding protein (SSB) sliding on untethered ssDNA substrate¹⁷. Our measurements recapitulated the rapid FRET fluctuations (Fig. 2b) previously observed using immobilized DNA substrates, and our measured rate $16.9 \pm 0.9\text{ s}^{-1}$ (Supplementary Fig. 6) is consistent with the previous measurement ($\sim 15\text{ s}^{-1}$, interpolated from ref. ¹⁷). In these two systems of relatively fast FRET dynamics,

ABEL-FRET also allows probing of the heterogeneity in the kinetic rates (Extended Data Fig. 4c and Supplementary Fig. 6). We further demonstrated that ABEL-FRET can monitor slower dynamics ($\sim 1\text{ s}^{-1}$) as exemplified by the binding and unbinding of RecA recombinase on a DNA substrate¹⁸ (Extended Data Fig. 5). These examples establish ABEL-FRET as a tether-free alternative to investigate intramolecular conformation dynamics from milliseconds to seconds.

Finally, we demonstrate hydrodynamic profiling: using single-molecule diffusivity, together with smFRET, to probe a two-dimensional space of molecule size and conformation. Before this work, hydrodynamic information in smFRET has been limited to (sub)ensemble averages over many molecules¹⁹. Profiling at the single-molecule level introduces many new exciting capabilities and we illustrate this with three examples. First, we probed Mg^{2+} -induced folding of the HJ. In the absence of Mg^{2+} ions, most HJs exhibit a constant FRET efficiency of ~ 0.3 (Fig. 2c). Previous gel electrophoresis²⁰ experiments suggest that the HJ exists in an extended conformation under this condition (no Mg^{2+}). Conventional smFRET, which only provides one-dimensional distance information (Fig. 2c marginal E_{FRET} histogram), is not able to directly test this model as a single value of FRET efficiency is consistent with many possible conformations. With ABEL-FRET, the additional diffusion coefficient (D) readout provides an unambiguous measure of the global compactness of each HJ. Indeed, when we plotted D together with

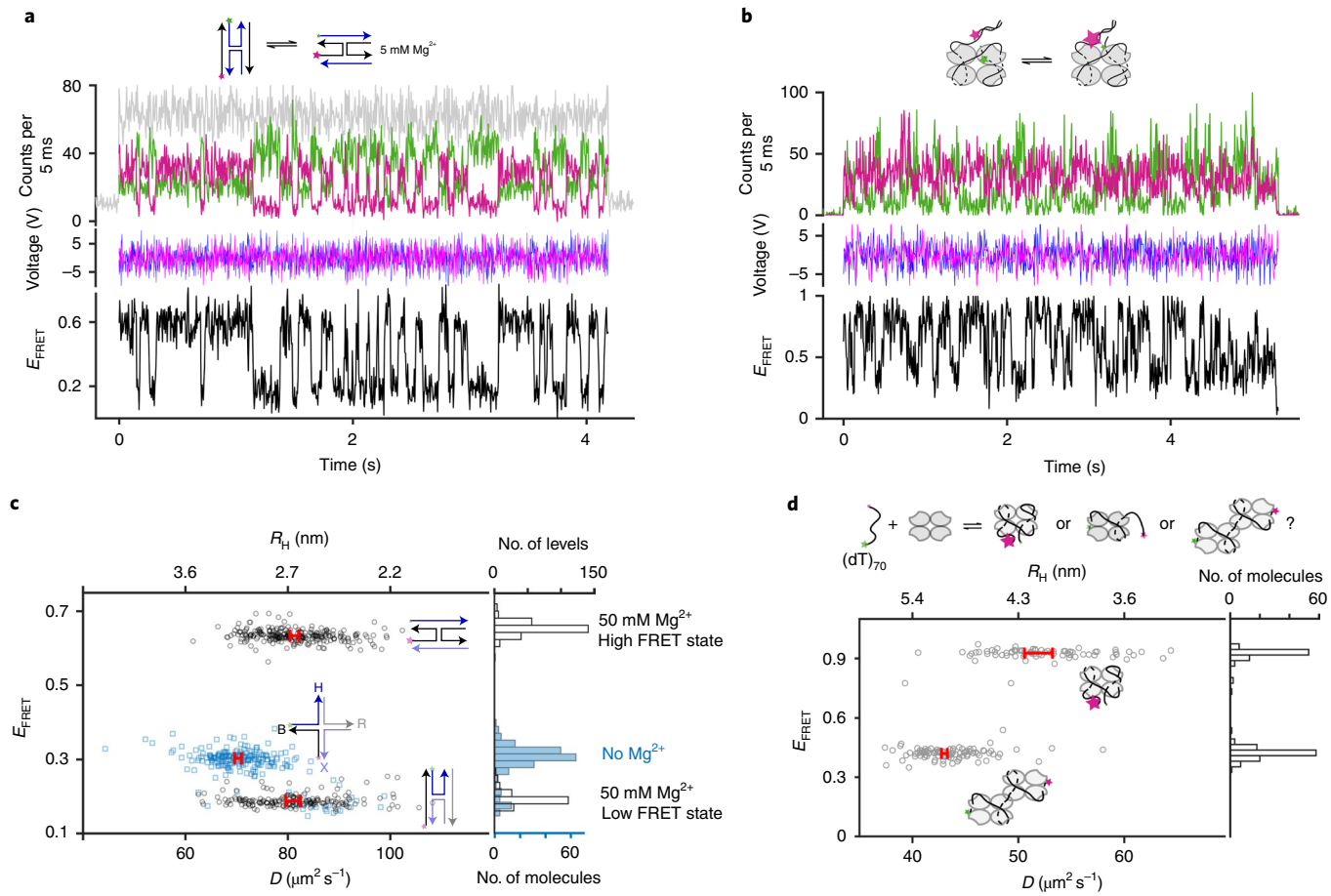


Fig. 2 | Tether-free smFRET dynamics and hydrodynamic profiling of biomolecules and their complexes. **a**, Example trace of a single HJ with 5 mM Mg^{2+} including fluorescence intensity (green, donor; red, acceptor; gray, total), feedback voltages and FRET efficiency. **b**, Top, SSB protein sliding on ssDNA causes rapid FRET fluctuations. Bottom, an example trajectory with 0.5 nM SSB , 200 mM NaCl . **c**, Probing Mg^{2+} -induced folding of HJs. Scatter plot of the diffusion coefficient (D) and FRET efficiency of identified FRET levels with a marginal E_{FRET} histogram. Light blue, no Mg^{2+} (0.5 mM EDTA); gray symbol, 50 mM Mg^{2+} . Red intervals indicate the uncertainties (95% confidence interval) in average D values of the respective populations. The hydrodynamic radii (R_h) were calculated from the diffusion coefficients using the Stokes-Einstein equation. **d**, Probing binding stoichiometry of SSB to ssDNA. Top, three possible binding configurations between SSB and ssDNA. Bottom, scatter plot of the diffusion coefficient (D) and FRET efficiency of 186 molecules with a marginal E_{FRET} histogram. Red intervals indicate the uncertainties (95% confidence interval) in average D (or R_h) values of the respective populations.

the efficiency of each FRET state, we observed that the ~ 0.3 FRET state (no Mg^{2+}) is associated with a lower D ($70.2 \pm 0.7\text{ }\mu\text{m}^2\text{ s}^{-1}$) while the two Mg^{2+} -induced isomers have similar and higher D (high FRET state, $81.3 \pm 0.9\text{ }\mu\text{m}^2\text{ s}^{-1}$; low FRET state, $80.9 \pm 1.4\text{ }\mu\text{m}^2\text{ s}^{-1}$, Supplementary Fig. 8). Further, these measured D values agree well with structure-guided hydrodynamic modeling of the extended and stacked states (Supplementary Note 7) and fluorescence correlation spectroscopy measurements (Supplementary Fig. 9). ABEL-FRET thus provides evidence at the single-molecule level that Mg^{2+} induces global compaction of HJ into two interconverting isomers²⁰.

As a second example, we used hydrodynamic profiling to determine the binding stoichiometry of SSB-ssDNA complexes²¹. On an ssDNA substrate (70 nucleotides (nt) in length, $(\text{dT})_{70}$), three binding scenarios are possible (Fig. 2d, top): one SSB tetramer fully wrapped with a footprint of 65 bases, one SSB tetramer partially wrapped with a footprint of 35 bases or two SSB tetramers on the ssDNA with each occupying 35 bases. Conventional smFRET revealed two populations in the end-to-end distance of the ssDNA with SSB bound (ref. ²¹, Fig. 2d marginal E_{FRET} histogram and Supplementary Fig. 7) but no direct information on binding stoichiometry. With a molecule-by-molecule, two-dimensional mapping of D and E_{FRET} (Fig. 2d and Supplementary Fig. 8),

ABEL-FRET clearly resolves that the low FRET state diffuses slower ($E \approx 0.45$, $D_{\text{mean}} = 43.0 \pm 0.3\text{ }\mu\text{m}^2\text{ s}^{-1}$) than the high FRET state ($E \approx 0.93$, $D_{\text{mean}} = 51.9 \pm 1.3\text{ }\mu\text{m}^2\text{ s}^{-1}$) and the difference can be fully accounted for by the hydrodynamic volume of a second SSB tetramer (Supplementary Note 7). We thus provide single-molecule evidence that the SSB exists in an equilibrium of two stoichiometric complexes on 70 nt of ssDNA: one SSB tetramer in the 65-nt binding mode or two SSB tetramers in the 35-nt binding mode.

As a third example, we show that concomitant smFRET and hydrodynamic profiling monitors the interplay between dynamic binding and conformation change of macromolecules in a multi-component reaction mixture, a task challenging for existing smFRET modalities. We created a DNA damage-repair cycle containing a substrate DNA, a nicking endonuclease that produces a specific 6-nt 5'-overhang and a polymerase that repairs the 5'-overhang using dNTP in solution (Fig. 3a and Supplementary Fig. 10). Here, the FRET pair on DNA reports the structural state of the substrate²²: damaged DNA shows $E_{\text{FRET}} \approx 0.7$ and fully repaired DNA shows $E_{\text{FRET}} \approx 0.5$ (Supplementary Fig. 11). Hydrodynamic profiling monitors the binding/unbinding of DNA-modifying enzymes, as binding induces a transient drop of diffusion coefficient from ~ 90 to $\sim 60\text{ }\mu\text{m}^2\text{ s}^{-1}$. The identity of a binding event (that is nicking

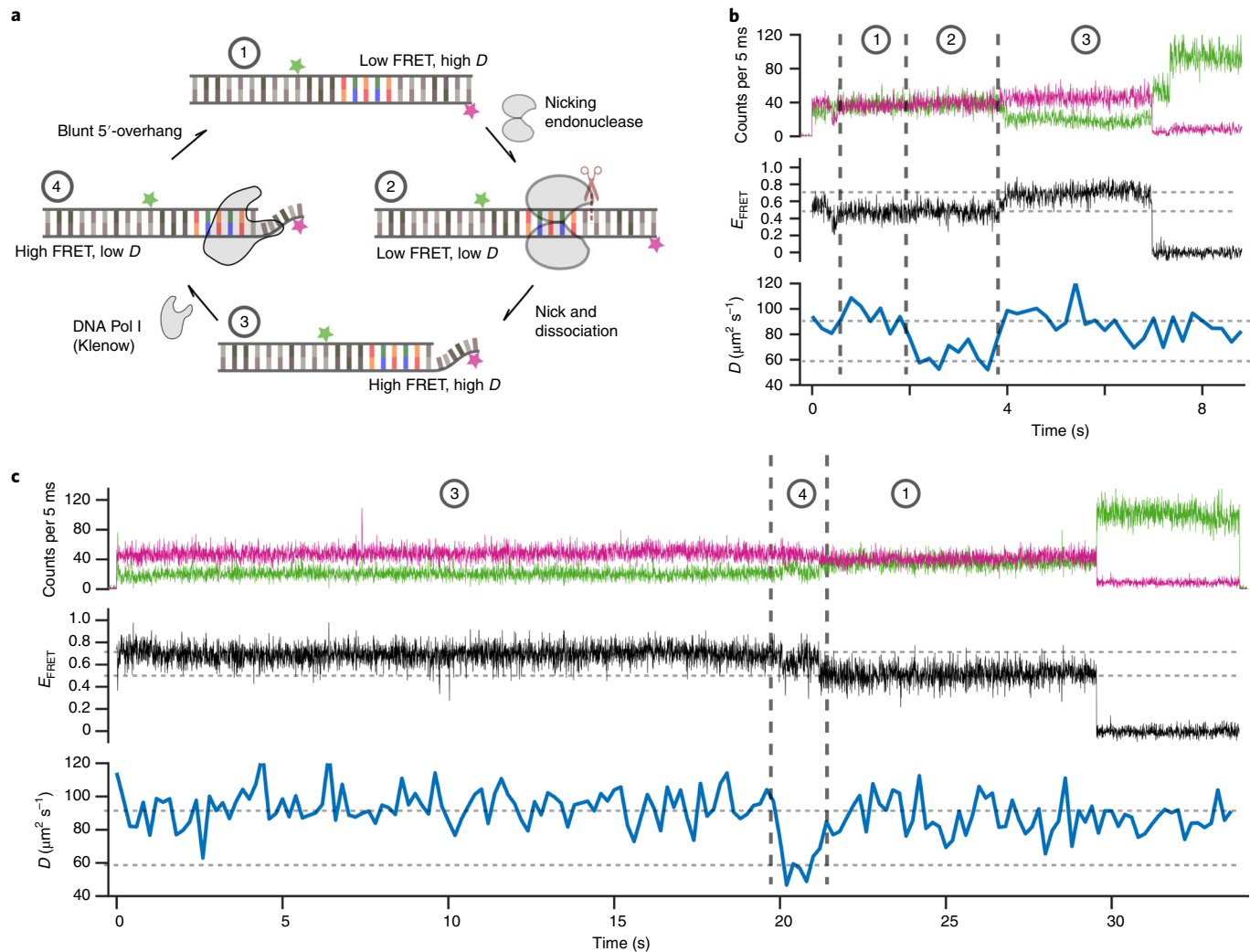


Fig. 3 | ABEL-FRET monitors single-molecule binding and conformational changes in a multi-component reaction mixture. **a**, Experimental scheme: a single DNA molecule goes through continuous nicking (damage) and polymerization (repair) cycles and its structural state (by FRET) and binding state (by hydrodynamic profiling) are monitored in real time. Circled numbers denote distinct states that can be resolved by ABEL-FRET using a combination of FRET state transitions and diffusion coefficient (D). **b**, An example trace showing nicking endonuclease binding (state 1 → 2), unbinding (state 2 → 3) and subsequent generation of damaged DNA (state 3). **c**, An example trace showing polymerase binding the damaged DNA (state 3 → 4), blunting the 5'-overhang (state 4) and unbinding (state 4 → 1) to yield the full DNA duplex (state 1). Vertical dashed lines denote the boundaries of identified states. Horizontal lines in E_{FRET} denote damaged (~0.7) and fully repaired DNA (~0.5). Horizontal lines in D denote free DNA (~90 $\mu\text{m}^2 \text{s}^{-1}$) and protein-bound DNA (~60 $\mu\text{m}^2 \text{s}^{-1}$).

endonuclease or polymerase) can be inferred from the effect on the substrate DNA (for example nicking produces damage, and thus a low-to-high FRET transition). With the DNA substrate, both enzymes and dNTPs in solution, ABEL-FRET successfully resolves DNA damage and repair steps (Fig. 3b,c and Extended Data Fig. 6) of the designed cycle, providing a unique single-molecule and DNA-centric view of a biochemical reaction containing three types of interacting biomolecules in real time. Several intriguing observations directly follow from this experiment. For one, almost every FRET change in the DNA was accompanied by a protein binding event shortly beforehand, but not all protein binding events altered DNA structure (Extended Data Fig. 6). For another, subtle FRET dynamics were observed when the polymerase is at work (at around 20 s in Fig. 3c and Extended Data Fig. 6), which may be reporting on mechanistic details of DNA polymerase^{23,24}. Lastly, fixing the 6-nt DNA damage sometimes requires multiple polymerase binding events (Extended Data Fig. 6h). Some events were not fully understood (for example at ~0.5 s in Fig. 3b), possibly due to the limited

time resolution (200 ms) of hydrodynamic profiling implemented here. With the ability to monitor binding and molecular conformation simultaneously, ABEL-FRET extends conventional smFRET to monitor structural dynamics in the proper context of biomolecular interactions and expands the complexity of biological problems that can be investigated.

In addition, ABEL-FRET naturally integrates excited-state lifetime measurements (Extended Data Fig. 7) and could be further enhanced by incorporating alternating-laser excitation²⁵ or pulsed interleaved excitation²⁶ (Supplementary Note 8) for accurate smFRET determination (required for distance measurements on biomolecules, Supplementary Note 5) and for checking acceptor photophysics.

Discussion

ABEL-FRET brings three major advances: tether-free observation of smFRET dynamics in solution, ultrahigh resolution of static structural heterogeneities and hydrodynamic profiling of

molecular compositions. ABEL-FRET does have some limitations compared to total internal reflection fluorescence microscopy (TIRF)-FRET, liposome encapsulation²⁷ and other smFRET modalities (Supplementary Table 1). Notably, the current observation time is limited to ~10 s, preventing slower dynamics on the minutes to hours²⁸ timescale from being directly monitored. Nevertheless, the work presented here brings new enabling capabilities for many smFRET investigations. With improved resolution, ABEL-FRET presents an opportunity to further advance smFRET-based refinement of biomolecular structures in solution^{29,30}. Additionally, simultaneous and independent probing of the hydrodynamic and conformational degrees of freedom allows clearer identification of molecular events and context, expanding the complexity of biochemical processes suitable for single-molecule investigations.

Online content

Any methods, additional references, Nature Research reporting summaries, source data, extended data, supplementary information, acknowledgements, peer review information; details of author contributions and competing interests; and statements of data and code availability are available at <https://doi.org/10.1038/s41592-021-01173-9>.

Received: 30 October 2019; Accepted: 4 May 2021;

Published online: 14 June 2021

References

- Ha, T. et al. Probing the interaction between two single molecules: fluorescence resonance energy transfer between a single donor and a single acceptor. *Proc. Natl Acad. Sci. USA* **93**, 6264–6268 (1996).
- Lerner, E. et al. Toward dynamic structural biology: two decades of single-molecule Förster resonance energy transfer. *Science* **359**, eaan1133 (2018).
- Rasnik, I., McKinney, S. A. & Ha, T. Surfaces and orientations: much to FRET about? *Acc. Chem. Res.* **38**, 542–548 (2005).
- Friedel, M., Baumketner, A. & Shea, J. E. Effects of surface tethering on protein folding mechanisms. *Proc. Natl Acad. Sci. USA* **103**, 8396–8401 (2006).
- Cohen, A. E. & Moerner, W. E. Method for trapping and manipulating nanoscale objects in solution. *Appl. Phys. Lett.* **86**, 093109 (2005).
- Dienerowitz, M., Howard, J. A. L., Quinn, S. D., Dienerowitz, F. & Leake, M. C. Single-molecule FRET dynamics of molecular motors in an ABEL trap. *Methods* <https://doi.org/10.1016/j.jymeth.2021.01.012> (2021).
- Heitkamp, T. & Börsch, M. Fast ATP-dependent subunit rotation in reconstituted FoF1-ATP synthase trapped in solution. Preprint at <https://arxiv.org/abs/2103.11986> (2021).
- Wang, Q. *Enabling Multivariate Investigation of Single-molecule Dynamics in Solution by Counteracting Brownian Motion* (Stanford University, 2014); <https://searchworks.stanford.edu/view/10689150>
- Wang, Q. & Moerner, W. E. Single-molecule motions enable direct visualization of biomolecular interactions in solution. *Nat. Methods* **11**, 555–558 (2014).
- Watkins, L. P. & Yang, H. Information bounds and optimal analysis of dynamic single molecule measurements. *Biophys. J.* **86**, 4015–4029 (2004).
- Holden, S. J. et al. Defining the limits of single-molecule FRET resolution in TIRF microscopy. *Biophys. J.* **99**, 3102–3111 (2010).
- Nir, E. et al. Shot-noise limited single-molecule FRET histograms: comparison between theory and experiments. *J. Phys. Chem. B* **110**, 22103–22124 (2006).
- Juette, M. F. et al. Single-molecule imaging of non-equilibrium molecular ensembles on the millisecond timescale. *Nat. Methods* **13**, 341–344 (2016).
- Tyagi, S. et al. Continuous throughput and long-term observation of single-molecule FRET without immobilization. *Nat. Methods* **11**, 297–300 (2014).
- Hanson, J. A. et al. Illuminating the mechanistic roles of enzyme conformational dynamics. *Proc. Natl Acad. Sci. USA* **104**, 18055–18060 (2007).
- McKinney, S. A., Déclais, A.-C., Lilley, D. M. J. & Ha, T. Structural dynamics of individual Holliday junctions. *Nat. Struct. Biol.* **10**, 93–97 (2003).
- Roy, R., Kozlov, A. G., Lohman, T. M. & Ha, T. SSB protein diffusion on single-stranded DNA stimulates RecA filament formation. *Nature* **461**, 1092–1097 (2009).
- Joo, C. et al. Real-time observation of RecA filament dynamics with single monomer resolution. *Cell* **126**, 515–527 (2006).
- Cristóvão, M. et al. Single-molecule multiparameter fluorescence spectroscopy reveals directional MutS binding to mismatched bases in DNA. *Nucleic Acids Res.* **40**, 5448–5464 (2012).
- Lilley, D. M. J. Structures of helical junctions in nucleic acids. *Q. Rev. Biophys.* **33**, 109–159 (2000).
- Roy, R., Kozlov, A. G., Lohman, T. M. & Ha, T. Dynamic structural rearrangements between DNA binding modes of *E. coli* SSB protein. *J. Mol. Biol.* **369**, 1244–1257 (2007).
- Fijen, C. et al. A single-molecule FRET sensor for monitoring DNA synthesis in real time. *Phys. Chem. Chem. Phys.* **52**, 541–553 (2017).
- Christian, T. D., Romano, L. J. & Rueda, D. Single-molecule measurements of synthesis by DNA polymerase with base-pair resolution. *Proc. Natl Acad. Sci. USA* **106**, 21109–21114 (2009).
- Berezhna, S. Y., Gill, J. P., Lamichhane, R. & Millar, D. P. Single-molecule Förster resonance energy transfer reveals an innate fidelity checkpoint in DNA polymerase I. *J. Am. Chem. Soc.* **134**, 11261–11268 (2012).
- Kapanidis, A. N. et al. Alternating-laser excitation of single molecules. *Acc. Chem. Res.* **38**, 523–533 (2005).
- Hendrix, J. & Lamb, D. C. Pulsed interleaved excitation: principles and applications. *Methods Enzymol.* **518**, 205–243.
- Sonnenfeld, A., Haran, G. & Boukobza, E. Immobilization in surface-tethered lipid vesicles as a new tool for single biomolecule spectroscopy. *J. Phys. Chem. B* **105**, 12165–12170 (2001).
- Zhuang, X. et al. Correlating structural dynamics and function in single ribozyme molecules. *Science* **296**, 1473–1476 (2002).
- Hellenkamp, B. et al. Precision and accuracy of single-molecule FRET measurements—a multi-laboratory benchmark study. *Nat. Methods* **15**, 669–676 (2018).
- Lerner, E. et al. FRET-based dynamic structural biology: challenges, perspectives and an appeal for open-science practices. *eLife* **10**, e60416 (2021).

Publisher's note Springer Nature remains neutral with regard to jurisdictional claims in published maps and institutional affiliations.

© The Author(s), under exclusive licence to Springer Nature America, Inc. 2021

Methods

ABEL-FRET setup. The ABEL trap was implemented based on a published design³¹ (Supplementary Fig. 1). Briefly, light from a 532-nm laser (Coherent Obis) was scanned by a pair of acousto-optic deflectors (AA Opto-electronic) to produce a 32-point ‘knight’s tour’ pattern at the sample plane ($\sim 3 \times 3 \mu\text{m}^2$). The scan speed was set to 600 ns per point, which achieves an effective imaging frame rate of $\sim 52 \text{ kHz}$. The molecule’s real-time position was estimated on a field programmable gate array (FPGA, National Instruments PCIe-7852R) with photon-by-photon mapping and a Kalman filter³² (Supplementary Fig. 1). Feedback voltage vectors were calculated using $\vec{V} = -g \hat{r}$, where \hat{r} is the filtered position estimate and g is a gain parameter (volts per micrometer of displacement). The voltages were applied to the microfluidic chip using a pair of $\times 20$ amplifiers (FLC F10AD) and platinum electrodes. The electric field strength in the trap was estimated assuming the voltage drops uniformly over a 100- μm region. The fluorescence signal was collected by a silicone oil immersion objective lens (Olympus UPLSAPO100XS, numerical aperture 1.35) and focused through a confocal pinhole (400 μm , Thorlabs) to restrict the detection volume. To enable smFRET detection, the signal after the pinhole was recollimated and spectrally separated into donor and acceptor paths using a dichroic beam-splitter (Semrock FF652-Di01-25 \times 36). The pass bands of the donor and acceptor channels were further narrowed by emission filters before photons were time-tagged by avalanche photodiodes (Laser Component Count T-100). The FPGA control program was modified to ensure that both donor and acceptor photons were used for feedback trapping. This was accomplished by combining the digital pulses generated by the two detectors (logical ‘or’ operation) before the position estimation step.

The laser power used in this work was 15–50 μW (measured at the back aperture of the objective), which corresponds to a power density of 180–600 W cm^{-2} at the sample (averaged over the $\sim 3 \times 3 \mu\text{m}^2$ laser scanning region). We note that both the laser power and power density used in ABEL-FRET are lower compared to burst-based confocal smFRET (power $\sim 100 \mu\text{W}$ (ref. ²⁹), peak density $\sim 8 \text{kW cm}^{-2}$), we thus do not expect laser-induced heating on the sample to be a unique issue for ABEL-FRET. To measure the time-resolved decay of the donor, excitation was provided by a spectrally filtered ($532 \pm 5 \text{ nm}$) supercontinuum fiber³³ (OFS Fitel) pumped by a mode-locked Ti:Sapphire oscillator (Mira 900, Coherent, tuned to 790 nm). Time-correlated single-photon counting was performed using a PicoHarp 300 module (PicoQuant). Excited-state lifetime was extracted using a maximum likelihood estimator as previously described³⁴.

Hydrodynamic profiling. The diffusion coefficient (D) of a trapped single molecule was estimated by a maximum likelihood approach developed previously⁹. Briefly, the in-trap motion is composed of diffusion and electrokinetic transport induced by the feedback electric voltages and sampled photon-by-photon with a localization uncertainty roughly equal to the size of the scanning laser beam. The algorithm uses an expectation-maximization framework to successively reconstruct the position trajectory of the molecule using a set of feedback voltages and known measurement error statistics and decomposes the displacements of the trajectory into a random and a voltage-dependent component. The diffusion coefficient is estimated from the random, voltage-independent parts of the displacements. In ABEL-FRET, the algorithm was modified to handle photon streams from two detector channels (Supplementary Software 2). In this work, D of a single molecule was estimated every 200 ms unless otherwise specified. These time-dependent D estimates were used to visualize protein binding events (Fig. 3) or averaged to yield the mean diffusivity of a single molecule (Fig. 2c,d). We showed previously⁹ that uncertainty in D estimation scales with $1/\sqrt{N}$, where N is the number of total photons detected (and also the number of position points of the motion trajectory because the position tracking is performed photon-by-photon). In this work, with 200-ms time resolution ($\sim 1,500$ –3,000 photons), a single D estimation has an uncertainty of $\sigma(D) \approx 0.1D$. For static systems (D constant during observation), the uncertainty can be decreased by averaging over many 200 ms, nonoverlapping data windows of a single molecule (or a FRET level) and further reduced by measuring an ensemble of identical single molecules (or levels) and calculating a population mean (Supplementary Fig. 8).

Microfluidic device fabrication, cleaning and passivation. The microfluidic devices used for ABEL-FRET experiments were fabricated in Princeton University’s Micro/Nano Fabrication Laboratory using a protocol modified from those published^{35,36} (Supplementary Note 1). To prevent nonspecific adsorption of the diverse array of DNA binding and processing enzymes in this work, we developed a simple and effective poly(ethylene glycol) (PEG) coating protocol tailored to the geometry of our microfluidic chambers. First, the device was cleaned by an overnight Piranha bath (3:1 mixture of sulfuric acid and hydrogen peroxide) followed by extensive rinsing with ultrapure water (18.2 MΩ). Next, the chip was incubated in 1 M potassium hydroxide for 15 min. Then, the interior of the chip was filled with mPEG-silane solution (Gelest SIM6492.73 or Laysan Bio MPEG-SIL-5000-1g, $>20 \text{ mg ml}^{-1}$ in 95% ethanol–5% water mixture with pH ~ 5)³⁷ and incubated for more than 24 h at room temperature. Finally, the chip was dried with pure nitrogen, flushed and stored in ultrapure water before use.

Sample preparation. Sequences of DNA samples are listed in Supplementary Tables 2 and 3. All strands were purchased from IDT, purified by high-performance liquid chromatography. For those that were labeled in house, the amine-modified strand was incubated with ~ 10 -fold excess of *N*-hydroxysuccinimide-functionalized dye (sulfonated Cyanine3 or sulfonated Cyanine5, Lumiprobe) in 0.2 M sodium bicarbonate buffer pH 8.3 for >4 h. The dye-labeled oligonucleotide was then purified using ethanol precipitation (three times) or size-exclusion columns (BioRad, P6, two times). The labeling efficiencies, determined by absorption measurements, were 70–90%. Duplex DNA was annealed by mixing the two complementary strands at $\sim 10 \mu\text{M}$ concentration in 20 mM HEPES pH 8 with 100 mM NaCl, heating to 95 °C for 2 min and slowly cooling (~ 4 h) to room temperature. HJs were annealed similarly in 25 mM HEPES pH 7.5 with 50 mM NaCl. The DNA samples were stored at -20°C before use.

All ABEL-FRET experiments were performed at $\sim 5 \text{ pM}$ of the labeled species in a trapping buffer containing 20 mM HEPES, 3 mM Trolox and an enzymatic oxygen scavenger system (50 nM protocatechuate-3,4-dioxygenase and 2.5 mM protocatechuic acid). Additional components were added depending on the experiments. Double-stranded DNA (dsDNA), 100 mM NaCl; HJ, 1, 5 or 50 mM MgCl₂ or 0.5 mM EDTA (no Mg²⁺); RecA, 100 mM NaCl, 10 mM MgCl₂, 1 μM RecA, 2 mM ATP or 1 mM ATPγS; (SSB)₆₅ sliding, 200 mM NaCl, 0.5 nM SSB; SSB binding stoichiometry, 40 mM NaCl, 10 nM SSB. DNA damage-repair cycle, 50 mM NaCl, 5 mM MgCl₂, 200 nM Nt.BsmAI, 1 nM Klenow fragment, 100 μM of each dNTP. Adenylate kinase, 50 mM NaCl and 2 mM MgCl₂. Sources of all reagents and protein samples are listed in Supplementary Table 4.

Data analysis. All data analysis was performed with customized software written in Matlab. First, data regions representing single molecules and background were extracted with the guide of a change-point finding algorithm^{38,39}. The mean background rates for the donor, acceptor and combined channels were then determined by fitting a Poisson distribution to the intensity histogram from the background regions. The apparent FRET efficiency of trapped molecules over time was determined with background and donor leakage correction, for every time bin or batch of N photons, using:

$$E_{\text{FRET}} = \frac{N_A}{N_A + N_D}$$

$$N_D = N_{\text{D},\text{total}} - B_D$$

$$N_A = N_{\text{A},\text{total}} - B_A - \alpha N_D$$

where $N_{\text{D},\text{total}}$ and B_D are the total and background counts on the donor channel, $N_{\text{A},\text{total}}$ and B_A are the total and background counts on the acceptor channel, and α is the leakage fraction (0.074, determined by analyzing donor-only dsDNA molecules). The γ correction, which takes into account the differences in quantum yield and detection efficiency between the donor and the acceptor¹⁹, was not included (except in Extended Data Fig. 7e, where it was determined from the anti-correlated steps in donor and acceptor intensity upon acceptor photobleaching using the equation $\gamma = \Delta I_A / \Delta I_D$). Molecules showing $E_{\text{FRET}} < 0.05$ were considered as donor only and not selected for further analysis except in Extended Data Fig. 7e, where the donor-only species was analyzed to extract τ_0 , the donor lifetime in the absence of FRET. FRET efficiency histograms were constructed on either a molecule-by-molecule basis or using a fixed number of photons as detailed in the main text. FRET histogram width was quantified by the standard deviation of a Gaussian fit. FRET state transitions in the HJ and RecA experiments were identified by a change-point finding algorithm with Gaussian statistics⁴⁰.

The intensity cross-correlation functions between the donor and acceptor channels were calculated and fit using an exponential function⁴¹:

$$\text{xcorr}(\tau) = A \exp(-k\tau)$$

where A and k are the two fitting parameters and τ is the time lag over which the correlation is calculated. Specifically, we calculate the intensity cross-correlation function using photon arrival times (as commonly done in fluorescence correlation spectroscopy), which preserves the highest achievable time resolution from fluorescence recordings. We used a flexible binning algorithm⁴², which allowed us to calculate the cross-correlation function on arbitrary time lag intervals (for example, either on a linear scale of 1–15 ms for HJ with 1 mM Mg²⁺, Extended Data Fig. 4a, or on a log scale from 50 μs to 0.5 s, Supplementary Fig. 9). The cross correlations were calculated on single-molecule data and then averaged over the molecules measured. For molecules that were trapped for more than 1 s, single-molecule rates were also determined (Extended Data Fig. 4c and Supplementary Fig. 6). In those single-molecule fits, a floating offset term (c_0) was included (full fitting function: $\text{xcorr}(\tau) = A \exp(-k\tau) + c_0$). Because ABEL-FRET records the arrival time of every detected photon, this photon-by-photon correlation analysis allows us to quantify dynamic processes that are faster than the 5-ms bin time used to display data.

Reporting Summary. Further information on research design is available in the Nature Research Reporting Summary linked to this article.

Data availability

All single-molecule raw data analyzed in this work are available at <https://doi.org/10.5281/zenodo.4716779>. Source data are provided with this paper.

Code availability

Instrument control and analysis codes used to collect and analyze the data during the current study are supplied as Supplementary Software.

References

31. Wang, Q. & Moerner, W. E. An adaptive anti-Brownian electrokinetic trap with real-time information on single-molecule diffusivity and mobility. *ACS Nano* **5**, 5792–5799 (2011).
32. Wang, Q. & Moerner, W. E. Optimal strategy for trapping single fluorescent molecules in solution using the ABEL trap. *Appl. Phys. B* **99**, 23–30 (2010).
33. Ranka, J. K., Windeler, R. S. & Stentz, A. J. Visible continuum generation in air–silica microstructure optical fibers with anomalous dispersion at 800 nm. *Opt. Lett.* **25**, 25 (2000).
34. Wang, Q. & Moerner, W. E. Lifetime and spectrally resolved characterization of the photodynamics of single fluorophores in solution using the anti-Brownian electrokinetic trap. *J. Phys. Chem. B* **117**, 4641–4648 (2013).
35. Cohen, A. E. & Moerner, W. E. Controlling Brownian motion of single protein molecules and single fluorophores in aqueous buffer. *Opt. Express* **16**, 6941 (2008).
36. Wood, S. L. et al. Revealing conformational variants of solution-phase intrinsically disordered tau protein at the single-molecule level. *Angew. Chem. Int. Ed.* **56**, 15584–15588 (2017).
37. Witucki, G. L. A silane primer: chemistry and applications of alkoxyl silanes. *J. Coat. Technol.* **65**, 57–60 (1993).
38. Watkins, L. P. & Yang, H. Detection of intensity change points in time-resolved single-molecule measurements. *J. Phys. Chem. B* **109**, 617–628 (2005).
39. Roy, R., Hohng, S. & Ha, T. A practical guide to single-molecule FRET. *Nat. Methods* **5**, 507–516 (2008).
40. Li, H. & Yang, H. Statistical learning of discrete states in time series. *J. Phys. Chem. B* **123**, 689–701 (2019).
41. Kim, H. D. et al. Mg²⁺-dependent conformational change of cRNA studied by fluorescence correlation and FRET on immobilized single molecules. *Proc. Natl Acad. Sci. USA* **99**, 4284–4289 (2002).
42. Laurence, T. A., Fore, S. & Huser, T. Fast, flexible algorithm for calculating photon correlations. *Opt. Lett.* **31**, 829 (2006).
43. Sorokina, M., Koh, H. R., Patel, S. S. & Ha, T. Fluorescent lifetime trajectories of a single fluorophore reveal reaction intermediates during transcription initiation. *J. Am. Chem. Soc.* **131**, 9630–9631 (2009).
44. Sanborn, M. E., Connolly, B. K., Gurunathan, K. & Levitus, M. Fluorescence properties and photophysics of the sulfoindocyanine Cy3 linked covalently to DNA. *J. Phys. Chem. B* **111**, 11064–11074 (2007).
45. Stennett, E. M. S., Ciuba, M. A., Lin, S. & Levitus, M. Demystifying PIFE: the photophysics behind the protein-induced fluorescence enhancement phenomenon in Cy3. *J. Phys. Chem. Lett.* **6**, 1819–1823 (2015).

Acknowledgements

We thank H. Li for preparation of the adenylate kinase sample, M. Lee for modeling the hydrodynamic property of the HJ, H. Yang for valuable feedback, J. Shaevitz for comments on an early version of the manuscript, E. Gatzogiannis for the loan of a Picoharp 300 unit, R. Windeler (OFS Fitel) for the generous gift of the photonic crystal fiber patch and the staff at Princeton's PRISM clean room (E. Mills, R. Akhmechet, Z. Lewicka and D. Barth) for assistance with ABEL trap fabrication. We also thank the laboratories of A. Amodeo and S. Shvartsman for access to their gel imager. This work was supported by the Lewis-Sigler Fellowship of Princeton University and US Department of Energy Office of Basic Energy Sciences and Photosynthetic Systems Grant DE-SC0002423.

Author contributions

H.W. and Q.W. designed the research, performed experiments and analyzed the data. H.W. wrote an initial draft of the manuscript. H.W. and Q.W. discussed and interpreted results and edited the manuscript.

Competing interests

The authors declare no competing interests.

Additional information

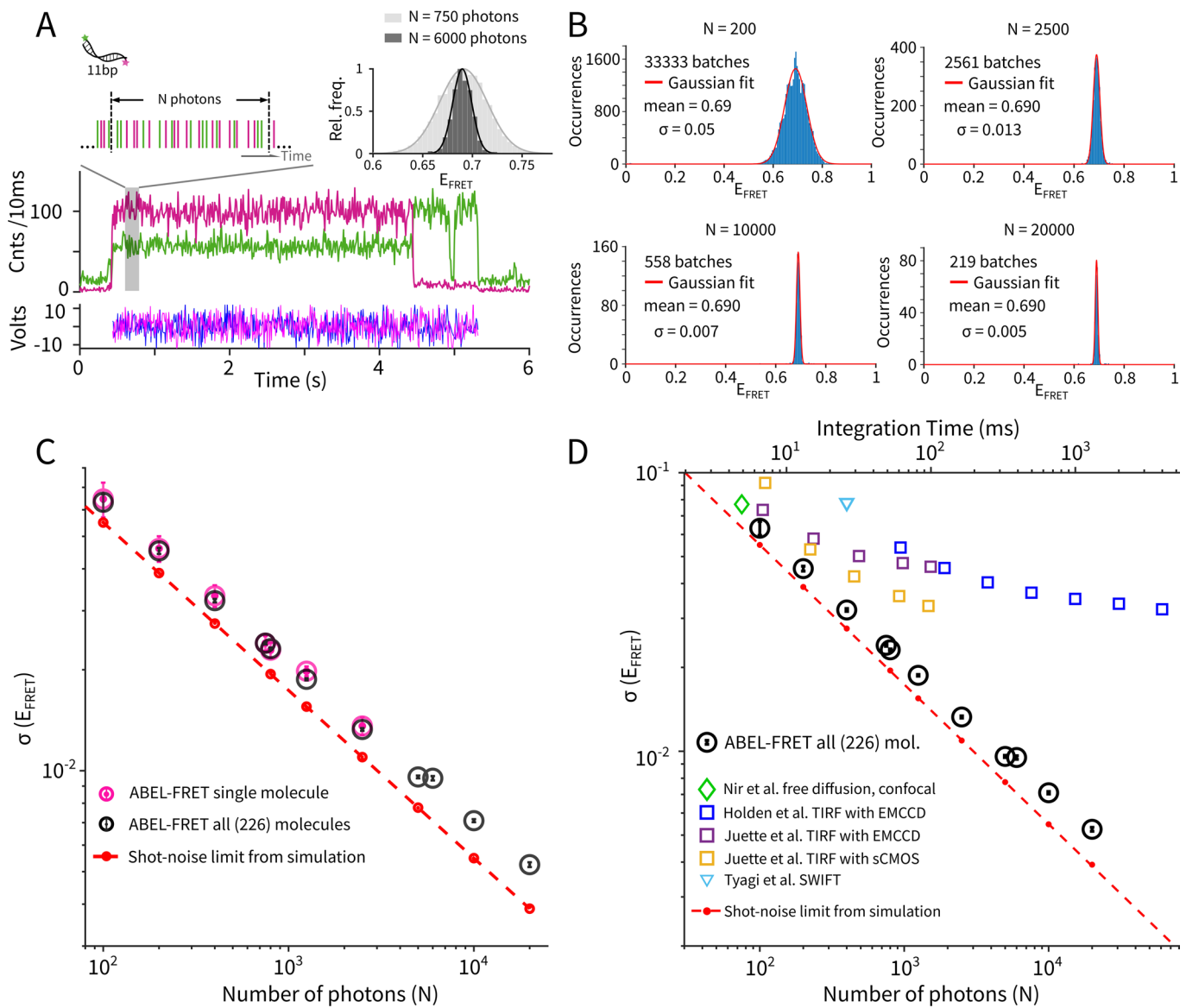
Extended data is available for this paper at <https://doi.org/10.1038/s41592-021-01173-9>.

Supplementary information The online version contains supplementary material available at <https://doi.org/10.1038/s41592-021-01173-9>.

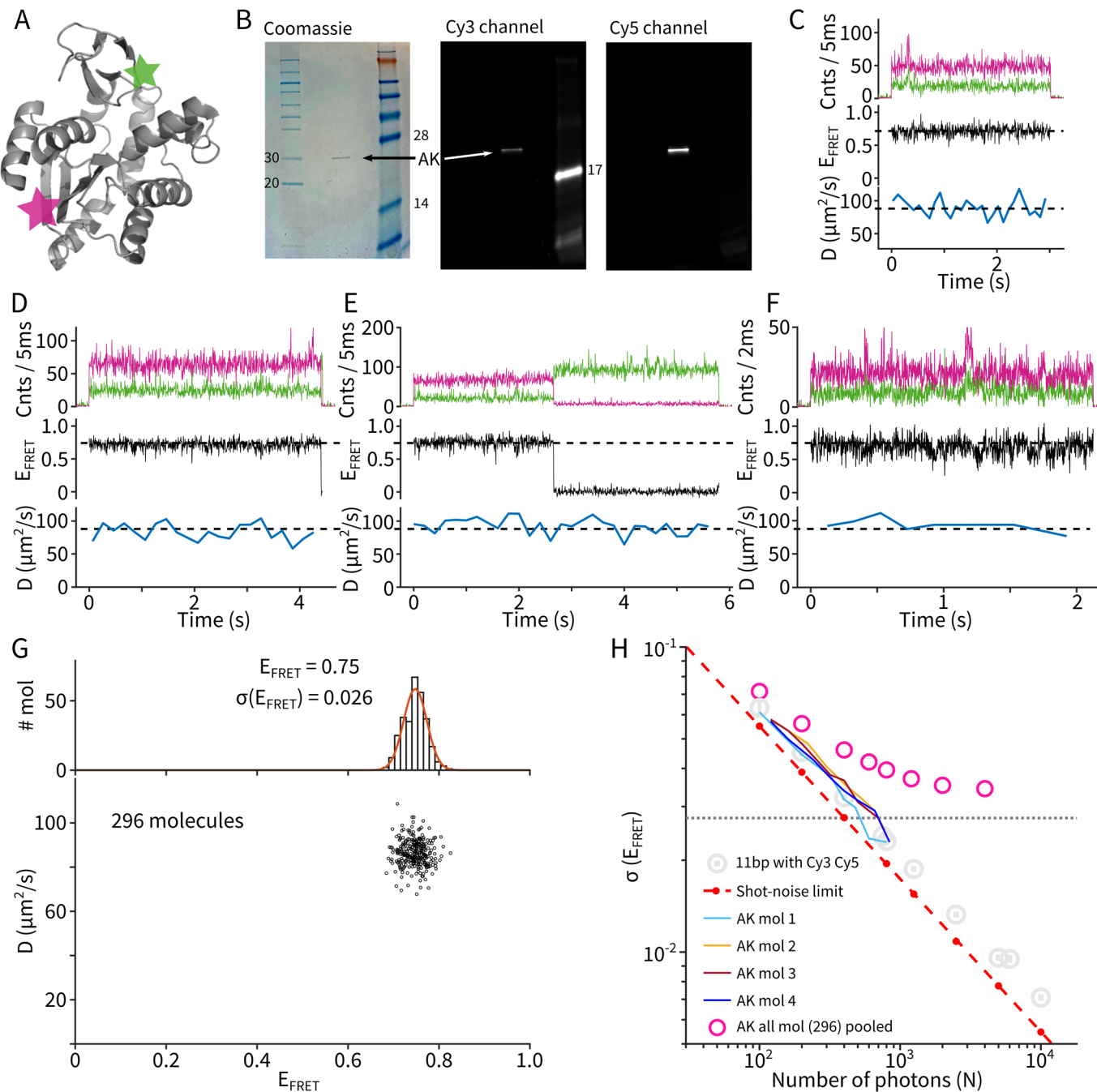
Correspondence and requests for materials should be addressed to Q.W.

Peer review information *Nature Methods* thanks Jens Michaelis and the other, anonymous, reviewer(s) for their contribution to the peer review of this work. Rita Strack was the primary editor on this article and managed its editorial process and peer review in collaboration with the rest of the editorial team.

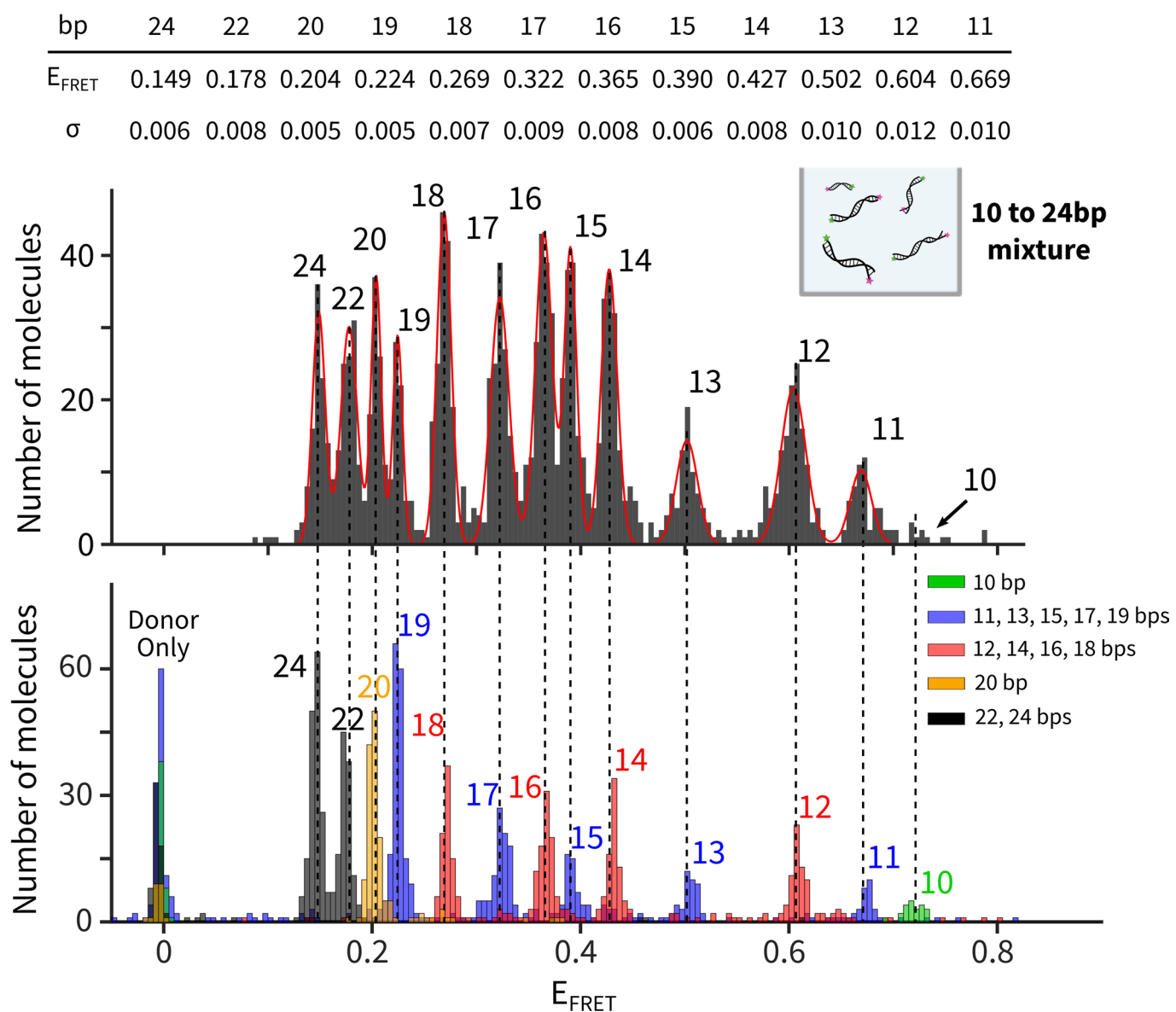
Reprints and permissions information is available at www.nature.com/reprints.



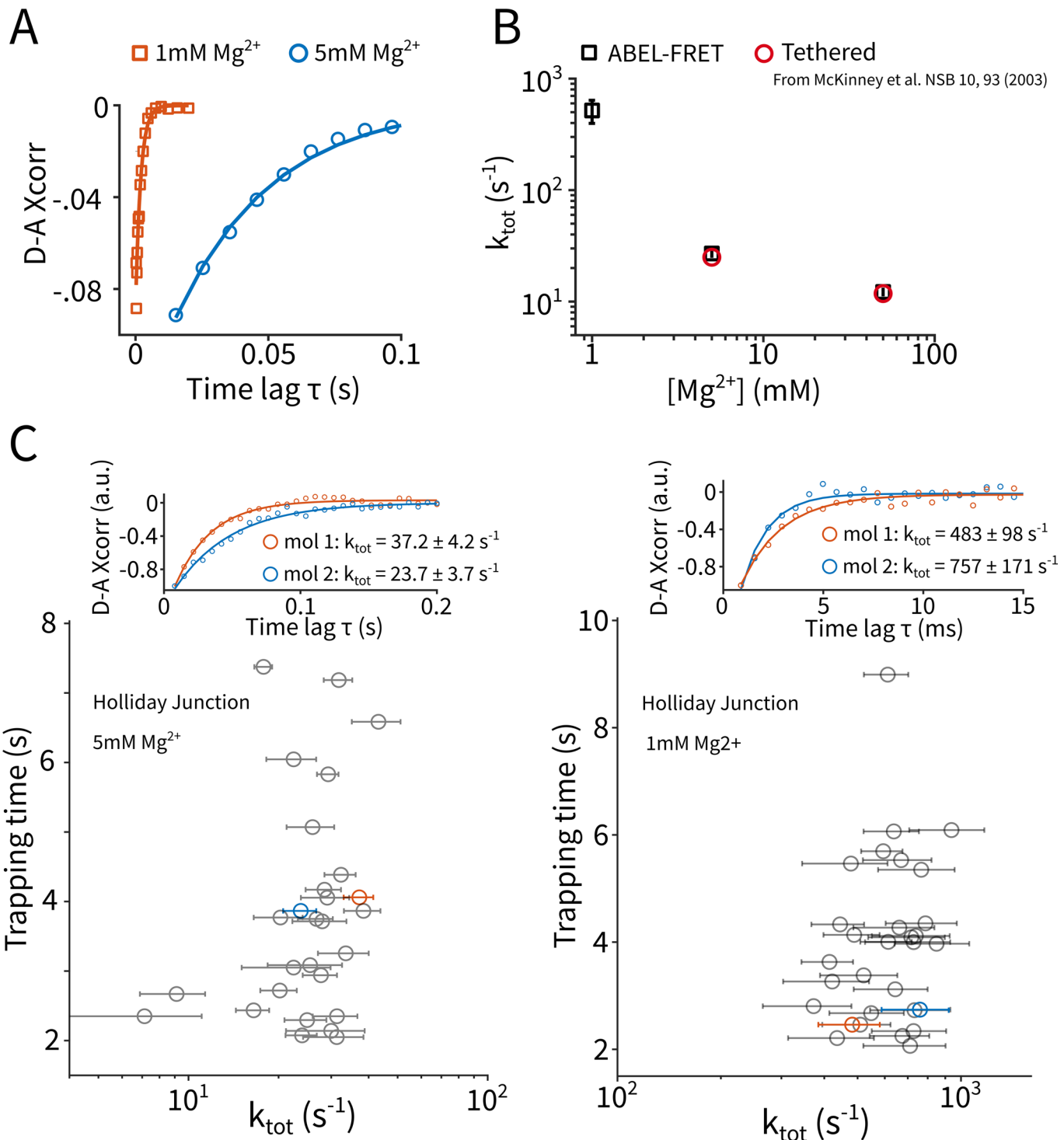
Extended Data Fig. 1 | Characterizing E_{FRET} histogram width of end-labeled 11bp dsDNA on the ABEL-FRET platform. **a**, Scheme: we divided a single trapping event into batches of N consecutive photons, calculated the FRET efficiency of each batch and constructed a histogram from data pooled from all measured molecules (a total of 226 molecules). We fit the resultant histogram using a Gaussian distribution and extracted the standard deviation (σ) to quantify histogram width. The inset shows example histograms constructed for $N = 750$ ($\sigma = 0.024$) and $N = 6000$ ($\sigma = 0.0095$). **b**, FRET histograms of the 11bp dsDNA sample for $N = 200$, 2500, 10000 and 20000. **c**, Histogram width as a function of N for data pooled from all (226) molecules (black symbol) and for one single molecule (magenta symbol). Red symbols represent the simulated shot-noise limit. Parameters used in the simulation were extracted from the 11 bp experiment: $E = 0.69$, $k_{D,s} + k_{A,s} = 13700 \text{ s}^{-1}$, $k_{D,b} = 1450 \text{ s}^{-1}$, $k_{A,b} = 238 \text{ s}^{-1}$. See Supplementary Note 2 for the definition of these parameters. Red dashed line denotes a linear fit to the simulated shot-noise limit. **d**, Comparing ABEL-FRET with other smFRET modalities. Integration time (top axis) is calculated from N using a measured detection rate of 15.4 kHz. Symbols mark literature values by different smFRET modalities. (Nir et al.: Ref. ¹²; Holden et al.: Ref. ¹¹; Juette et al.: Ref. ¹³; Tyagi et al. Ref. ¹⁴) Vertical errorbars in the ABEL-FRET dataset represent 95% confidence intervals for the fitted standard deviation (σ). We emphasize that the near shot-noise limited width in panel **c**, was obtained using the Cy3-Cy5 FRET pair (Supplementary Table 3). Other popular FRET pairs (for example Alexa488-Alexa594, Cy3B-Atto647N, etc) have yet to be characterized.



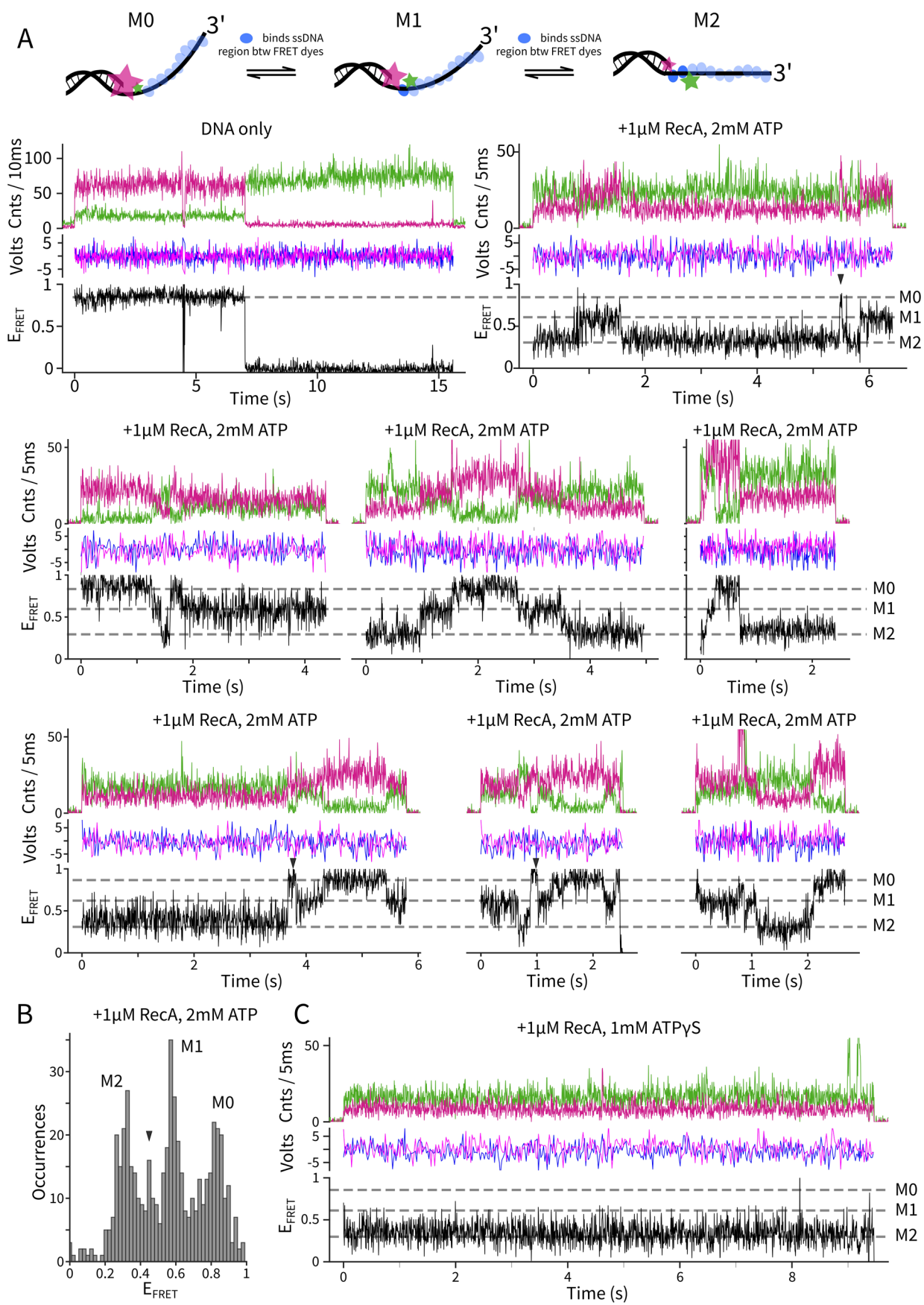
Extended Data Fig. 2 | ABEL-FRET achieves narrow smFRET histograms on the model protein adenylate kinase (AK). **a**, Structure and FRET labeling of E. Coli AK (PDB:1AKE). **b**, Sample validation: a single band consistent with the molecular weight of AK (~26 kDa) was observed on SDS-PAGE gel with fluorescence signal in both Cy3 and Cy5 channels. The gel images were obtained from a single experiment. **c-e**, Example ABEL-FRET traces of AK-Alexa555-Alexa647 without substrate. Most molecules show D values around $\sim 85 \mu\text{m}^2/\text{s}$, consistent with hydrodynamic modeling based on the crystal structure (Supplementary Note 7). About 4% of the molecules show much lower D values ($< 60 \mu\text{m}^2/\text{s}$, not shown). These were considered oligomers and excluded from further analysis even though FRET was observed. **f**, An example AK molecule in the presence of 0.5 mM AMP-PNP (adenosine 5'-[β,γ -imido]triphosphate, a nonhydrolyzable ATP analog) and 0.5 mM AMP showing frequent millisecond dynamics, similar to previously observed¹⁵. Note the intensity binning time is 2 ms in this example. **g**, Two-dimensional ($D-E_{\text{FRET}}$) distribution of 296 AK molecules measured without substrate and the corresponding FRET histogram. Each symbol represents D and E_{FRET} values averaged over a single AK molecule. Among these molecules, a mean of 16,200 photons were detected, lower than the experiment on Cy3-Cy5 labeled DNA (25,200 photons, Fig. 1c). **h**, The FRET histogram width $\sigma(E_{\text{FRET}})$ as a function of N for four single molecules (solid colored lines) and data pooled from 296 AK molecules (magenta circles). Data on 11 bp DNA (gray circles) and the corresponding shot-noise limit (red dashed line) are plotted as references. The horizontal dashed line ($\sigma = 0.026$) represents the width extracted from the molecule-by-molecule analysis in panel **G**. In this case, the single-molecule measurements were close to shot-noise limited but combining different molecules resulted in broadening in excess of the shot-noise limit. This is strong indication that molecule-to-molecule heterogeneity in this sample is responsible for the extra broadening.



Extended Data Fig. 3 | Validating the population identification of the 13-component DNA mixture experiment. Top: FRET histogram of the 13-component dsDNA experiment with a 12-component Gaussian fit. The mean and standard deviation of each population were extracted from the fit and tabulated. Note that the 10 bp DNA was included in the mixture but not well resolved (arrow), likely due to dissociation at the \sim pM concentration in the experiment. Bottom: individual measurements containing a specific subset of the mixture (see figure legend for details, each color represents one experiment). Dashed lines indicate good alignment between the samples. In the 13-component mixture experiment, it took a total of 283 minutes to acquire 1477 FRET-active molecules. The total data acquisition time includes molecule-by-molecule smFRET recording, waiting for new molecules to diffuse into the trapping region and measuring donor only molecules.

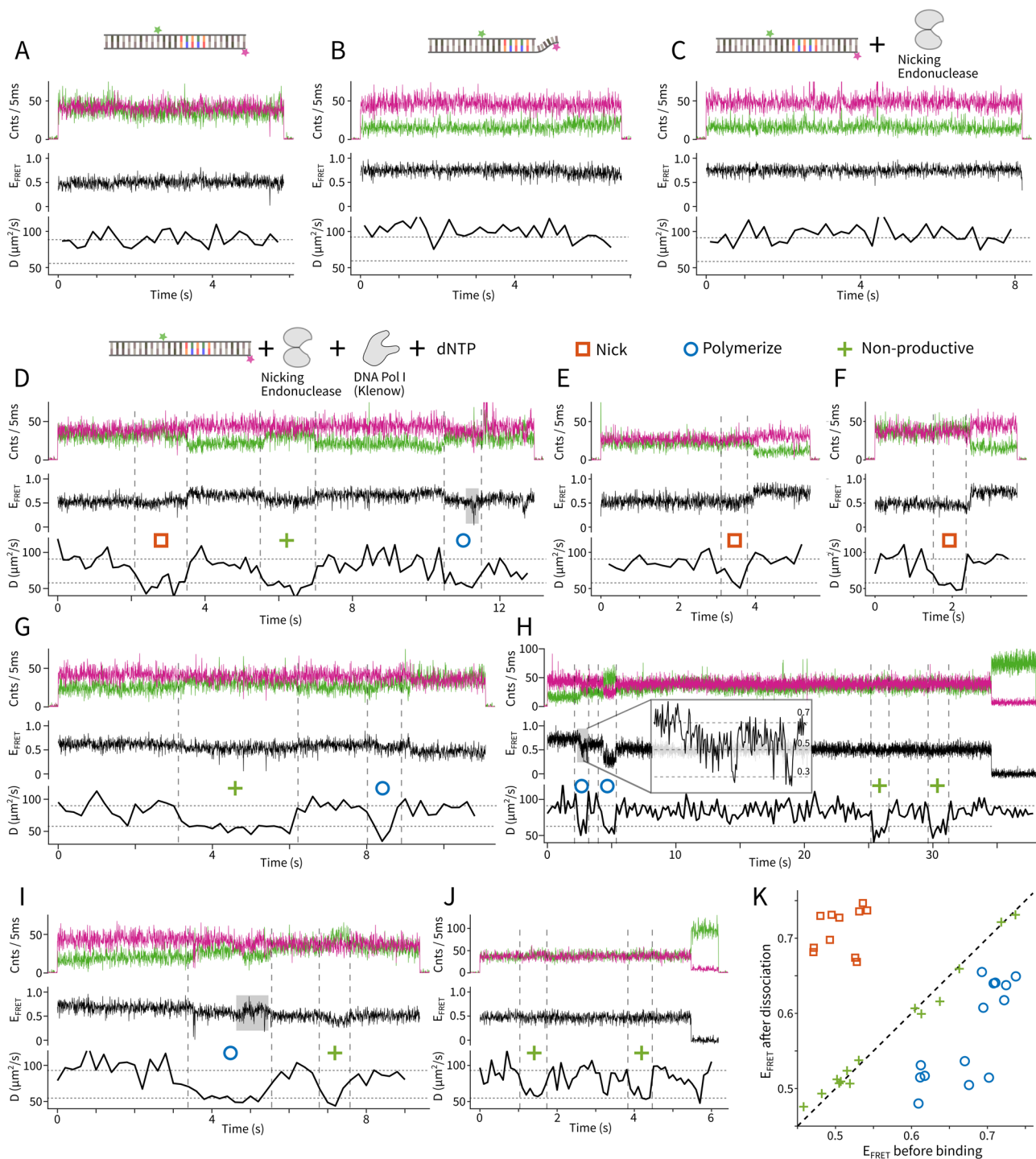


Extended Data Fig. 4 | Kinetic rates of Holliday junction dynamics. **a**, Donor-acceptor intensity cross-correlation curves of HJ for 1 mM Mg^{2+} (orange, averaged over 44 molecules) and 5 mM Mg^{2+} (blue, averaged over 59 molecules). Solid lines are single exponential fits. **b**, Extracted rates of HJ dynamics and comparison to literature values. Data are presented as fitted rates (k_{tot}) \pm 95% C.I. from the fits. **c**, Single-molecule rates of HJ dynamics. Example fits from two molecules (red and blue circles) are shown on the top for each condition (normalized to the peak amplitudes). In the scatter plots, data along the k_{tot} axis are presented as fitted rates \pm 95% C.I. from the fits. Further investigations are needed to determine if these apparent differences in k_{tot} are due to molecule-to-molecule heterogeneity or insufficient sampling of relatively short time traces.

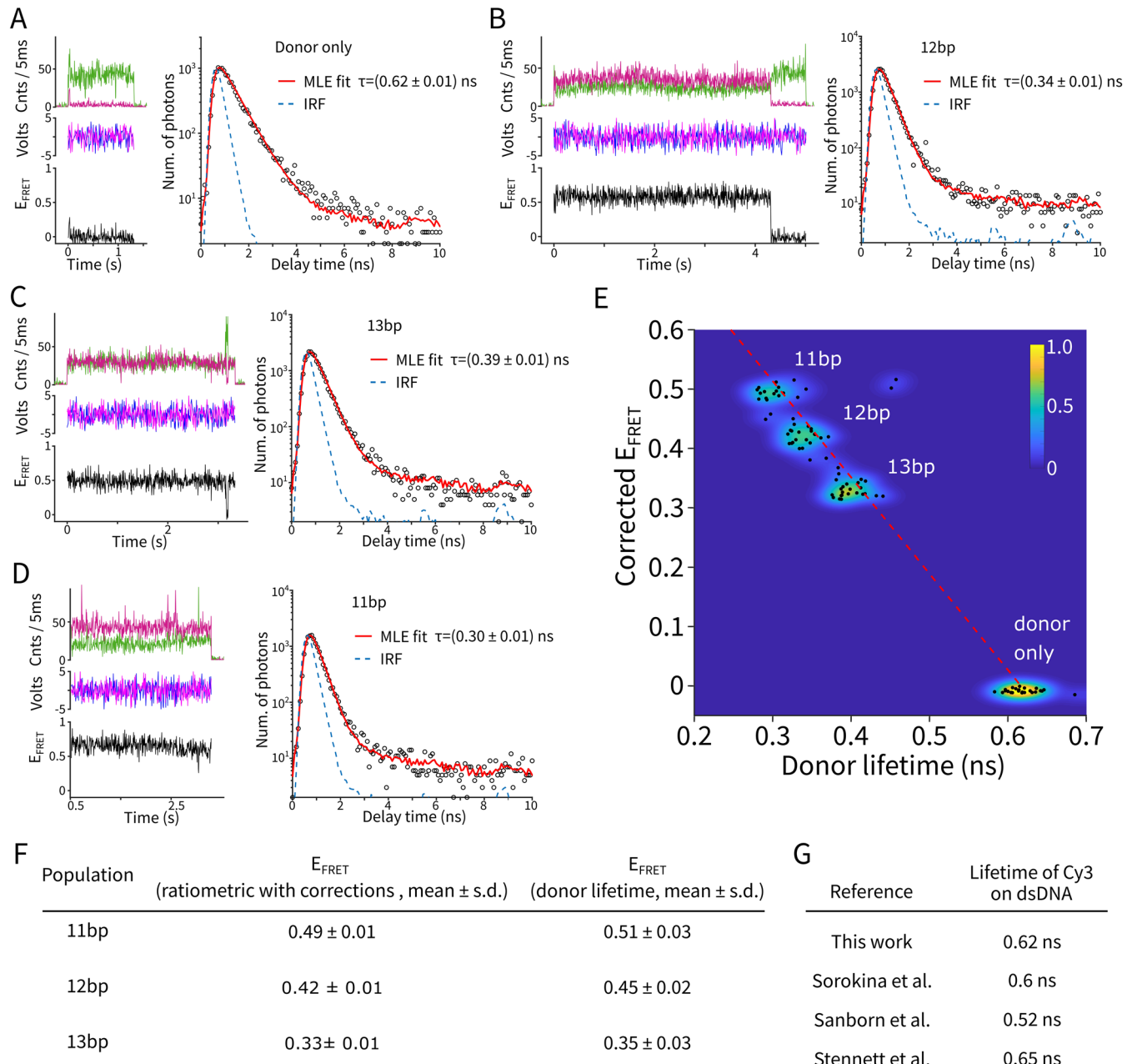


Extended Data Fig. 5 | See next page for caption.

Extended Data Fig. 5 | ABEL-FRET monitors slow ($\sim 1\text{s}^{-1}$) dynamics of the RecA-ssDNA nucleofilament. **a**, Top schematic: The experimental design is based on the smFRET assay developed in Ref. ¹⁸. The DNA sample is a partial duplex with a 60nt ssDNA overhang ((dT)₁₀₊₄₉). In the presence of ATP, the RecA protein subunits (blue ovals) are expected to bind the ssDNA overhang to form a nucleofilament that undergoes binding/unbinding dynamics near the dsDNA-ssDNA junction (that is the 5'-end of the ssDNA region). The FRET dyes are installed at the 5'-end of the ssDNA overhang to monitor distance changes induced by binding and unbinding of RecA protein. The separation between the FRET dyes is kept short (here 10 nt) to allow binding of only a few (here 2) RecA monomers between them. Additional RecA monomers cannot bind if the ssDNA region between the FRET pair has reached maximum occupancy (two monomers). Colored stars mark the positions of the FRET dyes. Blue ovals represent RecA monomers. Dark blue ovals mark RecA monomers that are bound in between the FRET dyes. Bottom: Example time traces under the conditions marked above each panel. We observed three major FRET states ($M_0 \sim 0.87$, $M_1 \sim 0.58$, $M_2 \sim 0.35$, horizontal dashed lines) and transitions between the three. These observations are similar to TIRF microscopy measurements on immobilized DNA substrates¹⁸ and were previously interpreted to represent RecA protein binding and unbinding. We also observed many transient ($<100\text{ ms}$) states (arrows) which could be missed in previous TIRFM measurements due to limited time resolution. **b**, Histogram of observed FRET levels, showing three major populations at M_0 , M_1 and M_2 and at least one possible minor state (arrow) at ~ 0.45 . Notably, our FRET efficiency histogram is much sharper compared to that obtained on immobilized molecules¹⁸. **c**, $(dT)_{10+49}$ in the presence of $1\mu\text{M}$ RecA and 1mM ATPyS only shows the M_2 state with no dynamics, representing the fully formed nucleofilament. This observation also agrees with previous experiments on immobilized DNA substrates¹⁸.



Extended Data Fig. 6 | More example ABEL-FRET traces that visualize the DNA damage-repair cycle. **a**, Substrate DNA only. **b**, Damaged DNA only. **c**, Substrate DNA incubated with nicking endonuclease. **d-j**, Substrate DNA with all components of the damage-repair cycle. Protein binding events were visualized by transient drops of diffusion coefficient. Three types of binding events were observed and annotated: binding that changes the E_{FRET} of DNA from low to high was identified to be nicking endonuclease damaging the DNA (orange squares), binding that changes the E_{FRET} of DNA from high to low was identified to be the polymerase repairing the damaged DNA (blue circles), binding that does not change E_{FRET} was considered non-productive (green plus signs). FRET fluctuations during polymerization events were frequently observed (shaded areas in panels D, H and I). Panel H shows an example trace that needed two consecutive (partial) polymerization runs (from 3–5.5 seconds, events marked with two blue circles) to completely repair. **k**, Mapping of observed binding events categorized by the structural consequences they induce on the substrate DNA.



Extended Data Fig. 7 | ABEL-FRET incorporates excited-state lifetime measurements. **a-d**, Example single-molecule traces showing intensity, feedback voltages, FRET efficiency and photon delay time histograms with fits. The sample is a mixture of 11 bp, 12 bp and 13 bp DNA duplexes. **e**, 2D scatter plot of corrected FRET efficiency versus donor lifetime. Black dots represent data acquired from single molecules. The underlying density is visualized using a 2D kernel density estimation algorithm. A total of 92 molecules were measured. The dotted red line shows the theoretical relationship $E = 1 - \tau/\tau_0$, where the value of τ_0 is extracted from the mean lifetime of the donor only species. **f**, E_{FRET} values calculated from intensity and lifetime-based measurements agree well. Background, donor leakage and γ corrections were applied to the intensity-based FRET calculation. **G**, Our measured lifetime of Cy3 on dsDNA is consistent with literature values. Sorokina et al.: Ref. ⁴³, Sanborn et al.: Ref. ⁴⁴, Stennett et al.: Ref. ⁴⁵.

Reporting Summary

Nature Research wishes to improve the reproducibility of the work that we publish. This form provides structure for consistency and transparency in reporting. For further information on Nature Research policies, see our [Editorial Policies](#) and the [Editorial Policy Checklist](#).

Statistics

For all statistical analyses, confirm that the following items are present in the figure legend, table legend, main text, or Methods section.

n/a Confirmed

- The exact sample size (n) for each experimental group/condition, given as a discrete number and unit of measurement
- A statement on whether measurements were taken from distinct samples or whether the same sample was measured repeatedly
- The statistical test(s) used AND whether they are one- or two-sided
Only common tests should be described solely by name; describe more complex techniques in the Methods section.
- A description of all covariates tested
- A description of any assumptions or corrections, such as tests of normality and adjustment for multiple comparisons
- A full description of the statistical parameters including central tendency (e.g. means) or other basic estimates (e.g. regression coefficient) AND variation (e.g. standard deviation) or associated estimates of uncertainty (e.g. confidence intervals)
- For null hypothesis testing, the test statistic (e.g. F , t , r) with confidence intervals, effect sizes, degrees of freedom and P value noted
Give P values as exact values whenever suitable.
- For Bayesian analysis, information on the choice of priors and Markov chain Monte Carlo settings
- For hierarchical and complex designs, identification of the appropriate level for tests and full reporting of outcomes
- Estimates of effect sizes (e.g. Cohen's d , Pearson's r), indicating how they were calculated

Our web collection on [statistics for biologists](#) contains articles on many of the points above.

Software and code

Policy information about [availability of computer code](#)

Data collection

Data was collected using custom software written in LabVIEW (National Instruments, version: 16.0f5, 32 bit) and Matlab (MathWorks, version: 9.1.0.441655, R2016b) on a computer running Windows 7 Professional (version 6.1, build: 7601, Service Pack 1). The custom instrument control and data acquisition software is provided as Supplementary Software 1

Data analysis

Data was analyzed using custom software written in Matlab (MathWorks, version 9.4.0.813654, R2018a) on a computer running Windows 7 Professional (version 6.1, build: 7601, Service Pack 1). The custom written Matlab software used for data analysis is provided as Supplementary Software 2

For manuscripts utilizing custom algorithms or software that are central to the research but not yet described in published literature, software must be made available to editors and reviewers. We strongly encourage code deposition in a community repository (e.g. GitHub). See the Nature Research [guidelines for submitting code & software](#) for further information.

Data

Policy information about [availability of data](#)

All manuscripts must include a [data availability statement](#). This statement should provide the following information, where applicable:

- Accession codes, unique identifiers, or web links for publicly available datasets
- A list of figures that have associated raw data
- A description of any restrictions on data availability

All single-molecule raw data analyzed in this work are available at <https://doi.org/10.5281/zenodo.4716779>.

Field-specific reporting

Please select the one below that is the best fit for your research. If you are not sure, read the appropriate sections before making your selection.

- Life sciences Behavioural & social sciences Ecological, evolutionary & environmental sciences

For a reference copy of the document with all sections, see nature.com/documents/nr-reporting-summary-flat.pdf

Life sciences study design

All studies must disclose on these points even when the disclosure is negative.

Sample size	The sample size was not predetermined. In each experiment enough data was collected to ensure that the sample size was large enough to make the statistical errors much smaller than the effect.
Data exclusions	We excluded a small number of data points (<5%) from Supplementary Fig. 2 due to anomalously high brightness. The full dataset with no exclusions also presented.
Replication	For each experiment the findings were reproduced successfully with similar results for at least two (2) times
Randomization	The random nature of molecule selection in each measured sample is intrinsic to the presented method
Blinding	Not relevant to this study since the work presents a novel single-molecule measurement scheme

Reporting for specific materials, systems and methods

We require information from authors about some types of materials, experimental systems and methods used in many studies. Here, indicate whether each material, system or method listed is relevant to your study. If you are not sure if a list item applies to your research, read the appropriate section before selecting a response.

Materials & experimental systems		Methods	
n/a	Involved in the study	n/a	Involved in the study
<input checked="" type="checkbox"/>	<input type="checkbox"/> Antibodies	<input checked="" type="checkbox"/>	<input type="checkbox"/> ChIP-seq
<input checked="" type="checkbox"/>	<input type="checkbox"/> Eukaryotic cell lines	<input checked="" type="checkbox"/>	<input type="checkbox"/> Flow cytometry
<input checked="" type="checkbox"/>	<input type="checkbox"/> Palaeontology and archaeology	<input checked="" type="checkbox"/>	<input type="checkbox"/> MRI-based neuroimaging
<input checked="" type="checkbox"/>	<input type="checkbox"/> Animals and other organisms		
<input checked="" type="checkbox"/>	<input type="checkbox"/> Human research participants		
<input checked="" type="checkbox"/>	<input type="checkbox"/> Clinical data		
<input checked="" type="checkbox"/>	<input type="checkbox"/> Dual use research of concern		